Geomechanics and Engineering, *Vol. 24, No. 6 (2021) 505-518*
DOI: https://doi.org/10.12989/gae.2021.24.6.505

Dynamic stability analysis of rock tunnels subjected to impact loading with varying UCS

Mohammad Zaid*

Department of Civil Engineering, Aligarh Muslim University, Aligarh, U.P. 202002, India

(Received September 21, 2020, Revised March 7, 2021, Accepted March 12, 2021)

Abstract. The present paper has been carried out to understand the effects of impact loading on the rock tunnels, constructed in different region corresponding to varying unconfined compressive strength (UCS), through finite element method. The UCS of rockmass has substantial role in the stability of rock tunnels under impact loading condition due to falling rocks or other objects. In the present study, Dolomite, Shale, Sandstone, Granite, Basalt, and Quartzite rocks have been taken into consideration for understanding of the effect of UCS that vary from 2.85 MPa to 207.03 MPa. The Mohr-Coulomb constitutive model has been considered in the present study for the nonlinear elastoplastic analysis for all the rocks surrounding the tunnel opening. The geometry and boundary conditions of the model remains constant throughout the analysis and missile has 100 kg of weight. The general hard contact has been assigned to incorporate the interaction between different parts of the model. The present study focuses on studying the deformations in the rock tunnel caused by impacting load due to missile for tunnels having different concrete grade, and steel grade. The broader range of rock strength depicts the strong relationship between the UCS of rock and the extent of damage produced under different impact loading conditions. The energy released during an impact loading simulation shows the variation of safety and serviceability of the rock tunnel.

Keywords: rock; unconfined compressive strength; finite element analysis; tunnel; impact loading

1. Introduction

The land insufficiency has raised the need for construction of underground structures for the transportation of goods & services and for storage of different materials (Pojani and Stead 2015). The tunnel has played an essential role as a part of underground structure as a metro, subway, water-tunnel, and sewage tunnel (Lane, 2019). Moreover, the use of tunnels for varying purposes in metro cities has aroused not only because of land scarcity; however, it has proved to be the medium of faster movement of people and other essential services in the region of dense population. The tunnels have been constructed in different medium that include low strength soil to high strength rocks. Therefore, the excavation, and construction of tunnels are being carried out by using bored tunnelling, cut-cover, shaft, box jacking, pipe jacking and other methods of construction. The study of tunnel stability has been an area of active research and different researchers had carried out studies related to the tunnels and its stability (Azizi *et al.* 2019, Naqvi *et al.* 2021, Wang and Cai 2020, Yang *et al.* 2019, Zhang *et al.* 2019, Zhao *et al.* 2019, Zaid and Sadique, 2021a,b).

Zhang *et al.* (2019) had studied the behaviour of rock tunnels by using visco-plastic deformation analysis to propose an analytical solution. They considered an auxiliary tunnel of hydropower plant for the validation of analytical results through an innovative fractional visco-plastic model (FVP-model), which has a spring, a visco-plastic body, and two-Abel dashpots. At first, the equation of creep was derived using von Mises plasticity for the FVP model. After that, the FVP model was modified through the combination of Hoek-Brown criterion and non-associated flow rule to derive a closed-form solution of the deformation of the rock. Kargar (2019) had also carried out the analytical study for the circular tunnels constructed in the rock mass. The solution proposed was for unlined tunnels, but both lined and unlined tunnels had proximity to the results when compared with the finite difference method. The coupled analytical solution had been proposed for deep circular tunnels by considering soft rock rheology and the advancement of tunnel face by Chu *et al.* (2019). The Lyon-Turin Base Tunnel had been considered to check the validity of the proposed solution. Several studies were also carried out for the study of tunnel stability in the rock mass (Do and Wu 2020, Huang *et al.* 2020, Liu *et al.* 2020, Park and Michalowski 2020, Rahaman and Kumar 2020, Rasmussen *et al.* 2019, Zareifard, 2020, Zaid and Mishra 2021, Zaid *et al.* 2019a, Zaid *et al.* 2020a).

The physical and mechanical strength of the rock mass has a significant role when the stability of the tunnel was studied. An exact solution for critical pressure had been investigated by Sofianos *et al.* (2006) through the Hoek-Brown criterion for rock tunnel. Moreover, they proposed a formula for the elastoplastic/elastic-brittle-plastic rock parameters in which tunnel has been constructed. Shrestha and Broch (2008) had studied the convergence of the underground rock tunnel considering the influence of morphology of the valley and rock mass strength. They

*Corresponding author, M.Tech Student
E-mail: mohammadzaid1@zhcet.ac.in

ISSN: 2005-307X (Print), 2092-6219 (Online)

used Phase2 numerical modelling software to explain the effect of morphology and rock strength. It was found that valley morphology, total height, and slope of valley induces the stress in the tunnel. They had concluded that the convergence in the weaker rock tunnel is more significant than the stronger rocks corresponding to the similar Q-values. The intermediate principal stress was found to be one of the influencing factors in rock mass strength resulting in a significant effect on the stress magnitude, and pressure in the rock tunnel (Huang *et al.* 2016). Moreover, the behaviour of tunnels in rocks concerning their inherent properties had been studied by several researchers (Abramson *et al.* 1993, Arias *et al.* 2016, Gurocak and Yalcin 2016, Lee 2012, McQueen *et al.* 2019, Qin *et al.* 2015, Shirlaw 2016, Song *et al.* 2011, Xia *et al.* 2020).

Researchers have also conducted studies on the behaviour of tunnels under the blast and impact loads (Buonsanti and Leonardi, 2013, Feldgun *et al.* 2008, Han *et al.* 2016, Koneshwaran *et al.* 2015, Kristoffersen *et al.* 2019, Li and Li 2018, Li *et al.* 2018, Shi *et al.* 2019, Xiang and Yang 2017, Yang *et al.* 2019, Zaid and Sadique, 2020a, b, Zhou *et al.* 2019, 2018, Han and Liu 2016, Jeon *et al.* 2015, Ozacar, 2018, Song *et al.* 2018, Uyar and Aksoy 2019, Zaid *et al.* 2019b, 2020b, 2021); and other failure modes in tunnels had also been studied (Chen *et al.* 2019, Kim and Park 2019). A submerged tunnel had been studied under an impact loading and it was concluded that the angle of the cable should be inclined between 45-degree to 60-degree (Xiang and Yang, 2017). Mishra *et al.* (2018) had carried the finite element analysis for different weathering stages of rock when subjected to the impact loading condition by using Abaqus. They concluded that the physical properties of the rock have a noteworthy role in the tunnel stability under impact loading and the deformations in the tunnel depends on the friction angle. Zhou *et al.* (2018) considered the propagation of cracks in the tunnel due to impact loading by using finite element and finite difference codes through Abaqus, and AUTODYN. They concluded that the propagation speed of cracks is not a constant quantity, but propagation may freeze for a period, which is defined as an arrest period. Further, this study was extended by defining two different modes of crack propagation (Zhou *et al.* 2019).

From the available literature, it has been found that tunnels constructed in the rocks have rarely been studied for impact loading conditions. Moreover, the finite element technique has also been rarely used for the impact loading on tunnels constructed in rocks. Furthermore, the relation between the strength specifically Unconfined Compressive Strength (UCS) of the rock and an impact load needs to be studied and discussed. Also, the effect of the grade of concrete and steel used in the tunnel lining had not been considered in the previous studies. Therefore, in this paper, the numerical modelling based study has been carried out using Abaqus for an impact loading on the tunnel that has been constructed in five different types of rocks. Different rocks have been considered to understand the correlation among the impacting load and the UCS of the rock surrounding the tunnel. Besides, four different types of concrete grades and three different grades of steel have been adopted for the concrete liner and its reinforcement, respectively. The present study highlights the behaviour of steel reinforcement, concrete lining and UCS of rock when the underground rock tunnel has been subjected to an impact loading condition.

2. Impact loading analysis

For carrying out the impact loading analysis in the present study, the Abaqus/Explicit code has been developed (Abaqus Systemes 2014). The geometry of the tunnel has dimensions of 30m x 30m in cross-section, and 35m of length of the tunnel. A 5 m diameter of the tunnel opening has been considered, and the concrete liner has 0.35m of thickness. The model has been considered based on boundary convergence study. From the DRMC specification, the steel reinforcement has been considered (Limited 2015). The reinforcement has two components; one is longitudinal, which has 10mm diameter steel bars at the spacing of 0.85m, and the second one is hoop reinforcement, which has been provided as two concentric reinforcements having 0.25m of spacing between them and 0.25m spacing along the longitudinal direction. The geometry of the whole model is shown in Fig. 1. Furthermore, the missile summed for the impact loading has been shown in Fig. 1(c), which has been taken from Vidanović *et al.* (2017).

The base of the rock surrounding the tunnel has been provided fixed support in all Cartesian directions. Moreover, right-left and front-rear sides (vertical) have been assigned roller support by allowing vertical movement of the rock. The missile has been assigned a velocity of 5000m/s and 100 kg weight. The embedment constraint has been assigned for the proper connection among the steel bars and the concrete liner. Also, the interaction between the liner, rock mass, missile, and reinforcement has been provided by applying general hard contact in the Abaqus. Further, the mesh convergence study has been carried out to maintain the accuracy of the results. The B31- element type meshes steel bars, which is defined as a two-node beam element and concrete liner, rock mass, and the missile has been meshed by the C3D8R-element type, which is the eight-node brick element having reduced integration and hourglass control.

2.1 Constitutive material modelling

The material model has been assumed isotropic, and the Mohr-Coulomb plasticity model is optimally suited to it. The Mohr-Coulomb model is given as follow:

$$\tau = \ c + \sigma \tan \phi \tag{1}$$

where, shear stress, cohesion, normal stress and friction angle are represented by τ, c, s, and ϕ respectively.

The model can also be represented in terms of three stress invariants to handle the general state of stress conveniently,

$$F = R_{mc} q - p \tan \phi - c = 0 \tag{2}$$

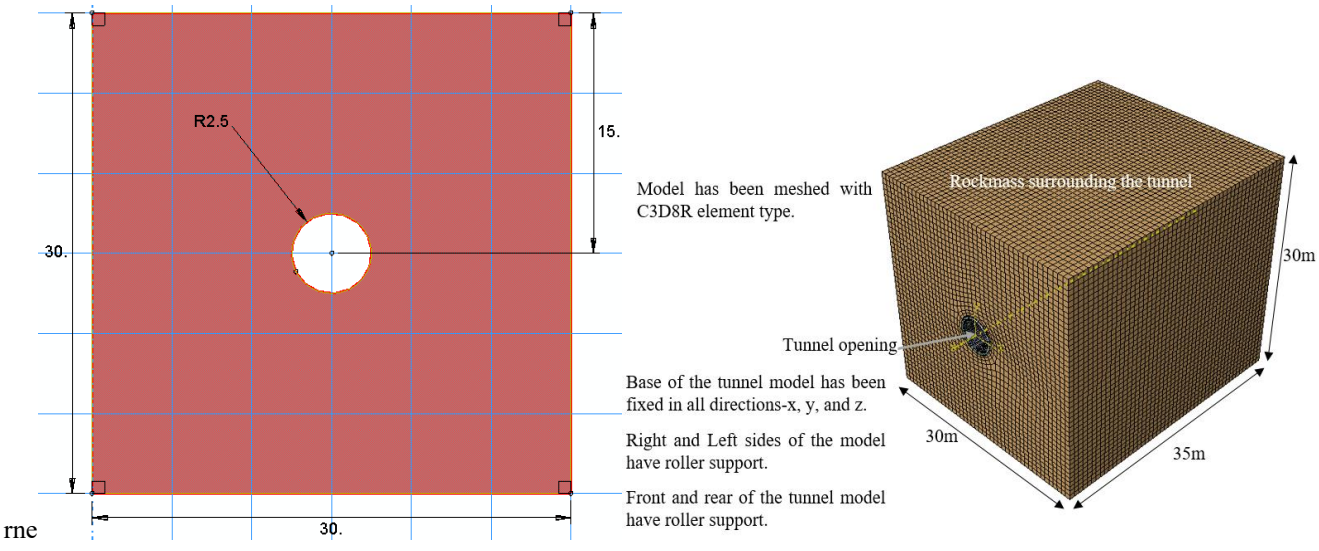

(a)

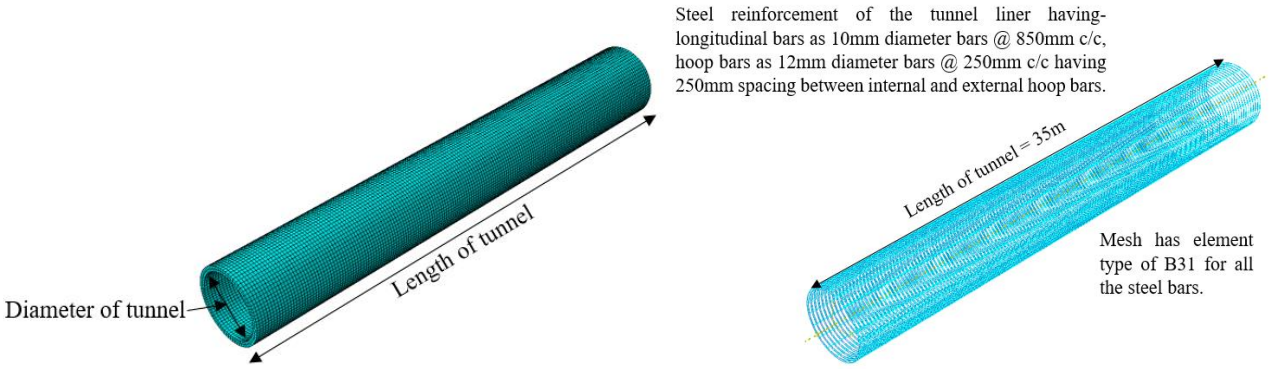

(b)

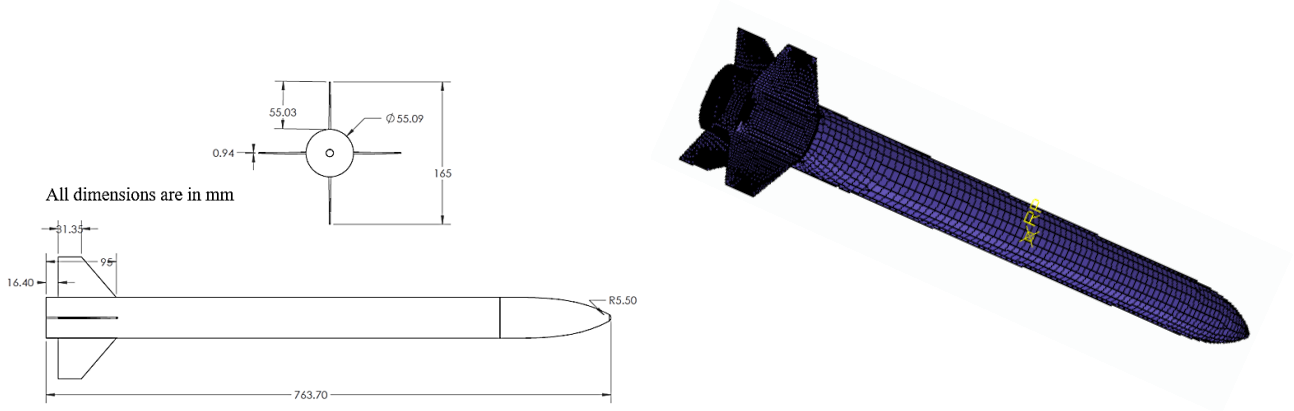

(c)

Fig. 1 Geometry, Meshing and Boundary condition adopted in the present study (a) Rock model, (b) Tunnel lining and (c) Impact Missile

where,

$$R_{mc}(\Theta,\phi) = \frac{1}{\sqrt{3}\cos\phi}\sin\left(\Theta+\frac{\pi}{3}\right)+\frac{1}{3}\cos\left(\Theta+\frac{\pi}{3}\right)\tan\phi \quad (3)$$

$$\cos(3\Theta) = \left(\frac{r}{q}\right)^3 \quad (4)$$

$$p = -\frac{1}{3}trace(\sigma) \quad (5)$$

$$q = \sqrt{\frac{3}{2}(S:S)} \quad (6)$$

$$r = (9(S*S:S))^{\frac{1}{3}} \quad (7)$$

$$S = \sigma + pI \quad (8)$$

where, deviatoric polar angle, equivalent pressure stress, Mises equivalent stress, third invariant of deviatoric stress,

Table 1 Properties of different rocks considered in the present study

Type of Rock	ρ (kg/m^3)	E (GPa)	ν	c (MPa)	ϕ	UCS (MPa)	Ref.
Dolomite	2160	08.12	0.230	03.36	25.22	02.85	(Gschwandtner and Galler 2013)
Shale	2550	12.50	0.250	16.00	27.00	50.90	(Kumar 2019)
Sandstone	2300	17.20	0.200	03.30	64.00	86.00	(Mitelman and Elmo 2014)
Granite	2750	36.84	0.187	25.23	58.32	132.80	
Basalt	2960	46.51	0.187	26.25	63.38	172.55	(Gupta 1997)
Quartzite	2680	93.75	0.185	27.13	65.30	207.03	

Table 2 Elasto-plastic properties of steel reinforcement (Goel *et al.* 2011)

Density (kg/m^3)	E (GPa)	Poisson Ratio	A (MPa)	B (MPa)	n	C	Strain Rate(s^{-1})
7800	210	0.3	360	635	0.114	0.075	100

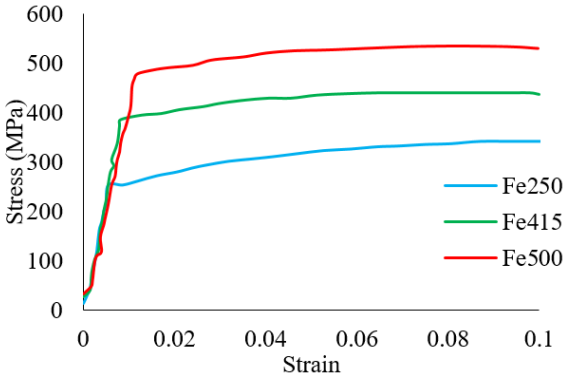

Fig. 2 Stress-strain behaviour of different steel grades (IS456, 2000)

and deviatoric stress are Θ, p, q, r, and S respectively.

Rate dependency hardening is not accounted for in this model. The flow rule G, for the Mohr-Coulomb model, is defined,

$$G = \sqrt{(\varepsilon c|_0 \tan\psi)^2 + (R_{mw} q)^2} - p\tan\psi \tag{9}$$

$$R_{mw}(\Theta, e) = \frac{4(1-e^2)\cos^2\Theta + (2e-1)^2}{2(1-e^2)\cos\Theta + (2e-1)\sqrt{4(1-e^2)\cos^2\Theta + 5e^2 - 4e}} R_{mc}\left(\frac{\pi}{3}, \phi\right) \tag{10}$$

$$R_{mc}\left(\frac{\pi}{3}, \phi\right) = \frac{3-\sin\phi}{6\cos\phi} \tag{11}$$

Dilation angle, cohesion yield stress, meridional eccentricity, and deviatoric eccentricity are represented by ψ, $c|_0$, ε, and $e = \frac{3-\sin\phi}{3+\sin\phi}$. The six different rocks having a varying range of UCS values considered in this study are Dolomite, Shale, Sandstone, Granite, Basalt, and Quartzite. The different parameters of the model are shown in Table 1.

The dynamic behaviour of steel bars used as reinforcement for tunnel lining have been modelled by Johnson-Cook (J-C) model, which is a type of isotropic hardening (Johnson and Cook 1983). The relation of the J-C model is given as follows,

$$\sigma^o = (A + B(\bar{\varepsilon}^{pl})^n)[1 + C\ln\left(\frac{\dot{\varepsilon}^{pl}}{\dot{\varepsilon}_0}\right)](1 - \hat{\theta}^m) \tag{12}$$

where, equivalent plastic strain, equivalent plastic strain rate, and reference strain state have been denoted by $\bar{\varepsilon}^{pl}$, $\dot{\varepsilon}^{pl}$ and $\dot{\varepsilon}_0$ respectively. Moreover, A, B, C, m, and n are the material parameters and $\hat{\theta}$ denotes the temperature defined as (homologous temperature),

$$\hat{\theta} \equiv \begin{cases} 0, for\ \theta < \theta_{transition} \\ \dfrac{(\theta - \theta_{transition})}{(\theta_{melt} - \theta_{transition})}, \quad for\ \theta_{transition} \leq \theta \leq \theta_{melt} \\ 1, \quad for\ \theta \geq \theta_{melt} \end{cases} \tag{13}$$

where, θ, θ_{melt}, and $\theta_{transition}$ denotes current temperature, melting temperature, and transition temperature. However, in the current study, the temperature-dependent stress-strain response is not considered. There are three different grades of steel reinforcement bars considered in the study, i.e., Fe250, Fe415, and Fe500 (IS456, 2000). Table 2 and Fig. 2 shows the input properties of the reinforcement.

The tunnel has been provided with a concrete lining that has been modelled by considering concrete damage plasticity (CDP) model (Hafezolghorani *et al.* 2015, Lubliner *et al.* 1989). The stress-strain relation of CDP model is given-

$$\sigma_t = (1 - d_t) D_0^{e1} : (\varepsilon - \varepsilon_t^{e1}) \tag{14}$$

$$\sigma_c = (1 - d_c) D_0^{e1} : (\varepsilon - \varepsilon_c^{e1}) \tag{15}$$

where, t and c refer to tension and compression respectively. σ, ε^{pl}, and d denotes the stress vector, plastic strain, and the damage variable respectively, D_0^{el} represents the undamaged elastic-stiffness (initial) of the material. The material damages in terms of elastic stiffness while unloading of concrete from any point, and this behaviour is described by damage variables. The damage variable value varies from 0 to 1 for the undamaged material to fully damaged material respectively. For this model, the yield function is given –

$$F = \left(\sqrt{\frac{3}{2}}\sqrt{:\bar{s}}\right) - 3\alpha\bar{p} + \beta\langle\hat{\bar{\sigma}}_{max}\rangle - \gamma\langle\hat{\bar{\sigma}}_{max}\rangle - (1-\alpha)\bar{\sigma}_c = 0 \tag{16}$$

Table 3 Input parameters of different grades of concrete (Hafezolghorani *et al.* 2015)

Concrete Grades	**M20**	**M30**	**M40**	**M50**
Density (kg/m^3)	2500	2500	2500	2500
Young's Modulus (GPa)	21.2	26.6	30.0	33.4
Poisson Ratio	0.2	0.2	0.2	0.2
Dilation Angle	31	31	31	31
Eccentricity	0.1	0.1	0.1	0.1
f_{b0}/f_{c0}	1.16	1.16	1.16	1.16
K	0.67	0.67	0.67	0.67
Viscosity Parameter	0	0	0	0

Table 4 Tension damage behaviour of different grades of concrete (Hafezolghorani *et al.* 2015)

Grades of Concrete	Concrete Tensile Behaviour		Concrete Tensile Damage	
	Yield Stress (MPa)	Cracking Strain	Damage Parameter	Cracking Strain
M20	2.00	0	0.00	0
	0.02	0.000943396	0.99	0.000943396
M30	3.00	0	0.00	0
	0.03	0.001167315	0.99	0.001167315
M40	4.00	0	0.00	0
	0.04	0.001333333	0.99	0.001333333
M50	5.00	0	0.00	0
	0.05	0.001494322	0.99	0.001494322

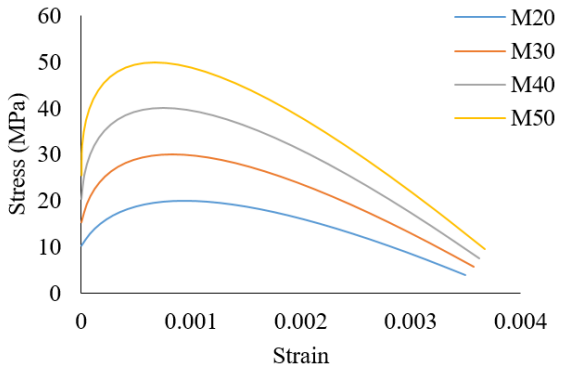

Fig. 3 Stress-strain graph of different concrete grades (Hafezolghorani *et al.* 2015)

where,

$$\alpha = \frac{\left(\frac{\sigma_{b0}}{\sigma_{c0}}\right) - 1}{2\left(\frac{\sigma_{b0}}{\sigma_{c0}}\right) - 1} \tag{17}$$

$$\beta = \frac{\bar{\sigma}_c}{\bar{\sigma}_t}(1-\alpha) - (1+\alpha) \tag{18}$$

$$\gamma = \frac{3(1-K_c)}{2K_c - 1} \tag{19}$$

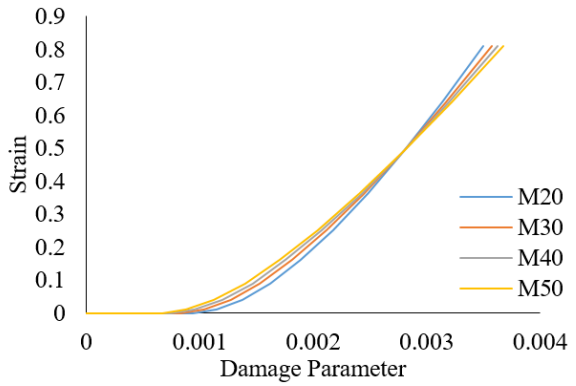

Fig. 4 Compressive Damage Parameter-strain graph of different grades of concrete (Hafezolghorani *et al.* 2015)

$$\bar{\sigma}_c = \frac{\sigma_c}{(1-d_t)} \tag{20}$$

$$\bar{\sigma}_t = \frac{\sigma_t}{(1-d_t)} \tag{21}$$

where, maximum effective principal stress, deviatoric stress tensor, and ratio of initial equi-biaxial to uniaxial compressive yield stress are denoted by $\hat{\bar{\sigma}}_{max}$, $\bar{s}$, and $\frac{\sigma_{b0}}{\sigma_{c0}}$ respectively. The plastic potential function G is

$$G_P = \sqrt{(\varepsilon\sigma_{t0}\tan\psi)^2 + \left(\frac{3}{2}s{:}s\right)} - \bar{p}\tan\psi \tag{22}$$

where, ψ, $\sigma_{t0}$and ε represents the dilation angle, uniaxial tensile stress and eccentricity respectively. This flow potential, which is continuous and smooth, ensures that the flow direction is defined uniquely. Four different grades of concrete are considered in the study, i.e., M20, M30, M40, and M50 (Hafezolghorani *et al.* 2015). The properties of these different grades of concrete are shown in Table 3, Table 4, Figs. 3 and 4 (Hafezolghorani *et al.* 2015).

3. Validation

The validation has been carried out using finite element modelling of rock mass models subjected to impact loading. The finite element software Abaqus has been used. Extensive numerical modelling was carried out for assessing deformations at different locations of lining under varying cover depth and drop energies. Rock and tunnel geometry has been created using the lagrangian analysis option in Abaqus explicit code to fully consider the three-dimensional effects of the 3D finite element model, which is based on a continuum approach

Three-dimensional finite element models of rock samples having its size 30 cm (Height) x 30 cm (Width) x 35cm (Length), with tunnel having the cover depth of 25 mm, 35 mm and 50 mm, has been used as a target of a drop hammer. Rigid hammers of different masses have been freely dropped from the height of 1.12 m, similar to the tests carried out in the laboratory by Sharma *et al.* (2018). In each case, the hammer acted as an impact for hitting the

Table 5 Properties of different material used in the validation of a numerical model (Mishra 2019)

Material Types	Elasticity Modulus (GPa)	Poisson's Ratio (ν)	Density (kg/m^3)	Friction Angle	Cohesion (MPa)	UCS (MPa)
SM	2.81	0.216	1093.90	31.40	0.627	1.97
POP	4.48	0.220	1170.00	51.00	0.780	6.78
PVC	3.000	0.400	1400.00	-	-	-

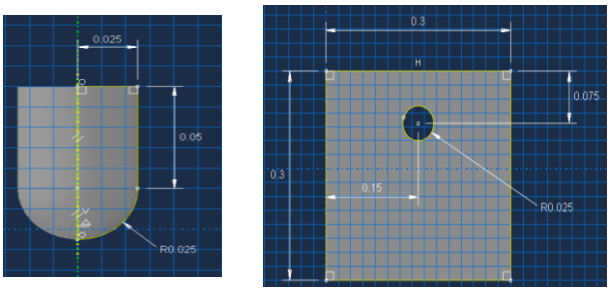

(a) (b)

Fig. 5 (a) Geometry of the Hammer and (b) Geometry of Tunnel Model

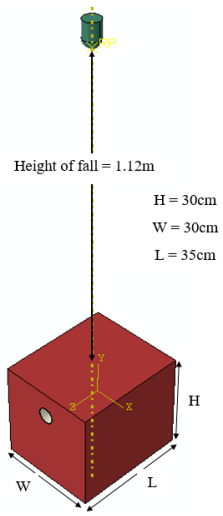

Fig. 6 Assembly, loading and Boundary conditions

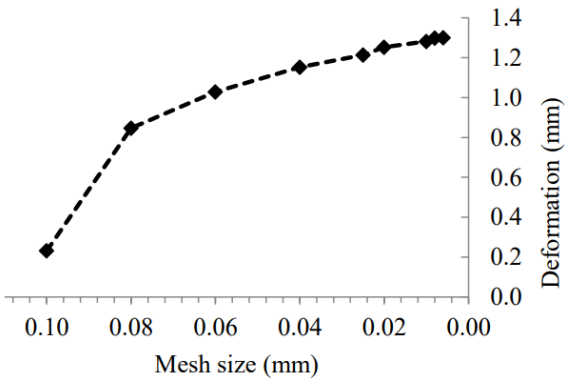

Fig. 7 Mesh Convergence

targets. Therefore, in this study, the assumption of the tricking condition has been taken into account, which reflects the practical study in most cases. Besides, air

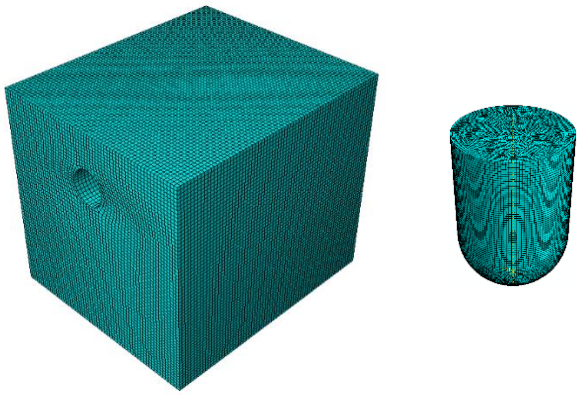

(a) (b)

Fig. 8 Meshing of (a) Tunnel model and (b) Hammer model

Table 6 Validation of impact loading on tunnels (Sharma *et al.* 2018)

Type of material	Overburden depth	Drop Hammer	Deformation at Crown of Tunnel (mm)	
			Experimental Study	*Numerical Study (Present)*
SM	25 mm	7.4	1.244	1.331
		10.0	1.775	1.908
	35 mm	7.4	0.314	0.334
		10.0	0.863	0.949
	50 mm	10.0	0.175	0.186
		12.4	0.353	0.378
POP	25 mm	10.0	0.934	1.055
		12.4	1.265	1.353
	35 mm	12.4	0.625	0.675
		15.0	0.703	0.759
	50 mm	12.4	0.226	0.241
		17.6	0.421	0.456

resistance has been neglected, i.e., at the time of impact loading, drop hammer has velocity equal to 4.68 m/sec, and total energy in hammer is in the form of kinetic energy. The drop hammer takes approximately 0.47 sec time to reach the target model on free falling from a specific height. The section sketches of the hammer and the rock model having overburden as 50 mm is shown in Fig. 5.

Various experimental tests have been done to get basic properties of the synthetic mix in laboratory and properties used as an input parameter in Abaqus, which shows the uniqueness of each material (Mishra 2019). The Mohr-Coulomb plasticity model is used for modelling the rock mass. The properties of Synthetic rock material (SM), Plaster of Paris (POP) and PVC lining have been taken for numerical simulation, as shown in Table 5.

The dimensions of the rock model has 5 cm diameter tunnel in the domain of 30 cm x 30 cm cross-section extruded by 35 cm in length at an overburden depth of 25 mm, 35 mm and 50 mm from the top surface of the model. The hammer is given a free fall under a gravitational effect from a height of 1.12 m (Mishra 2019). The model is

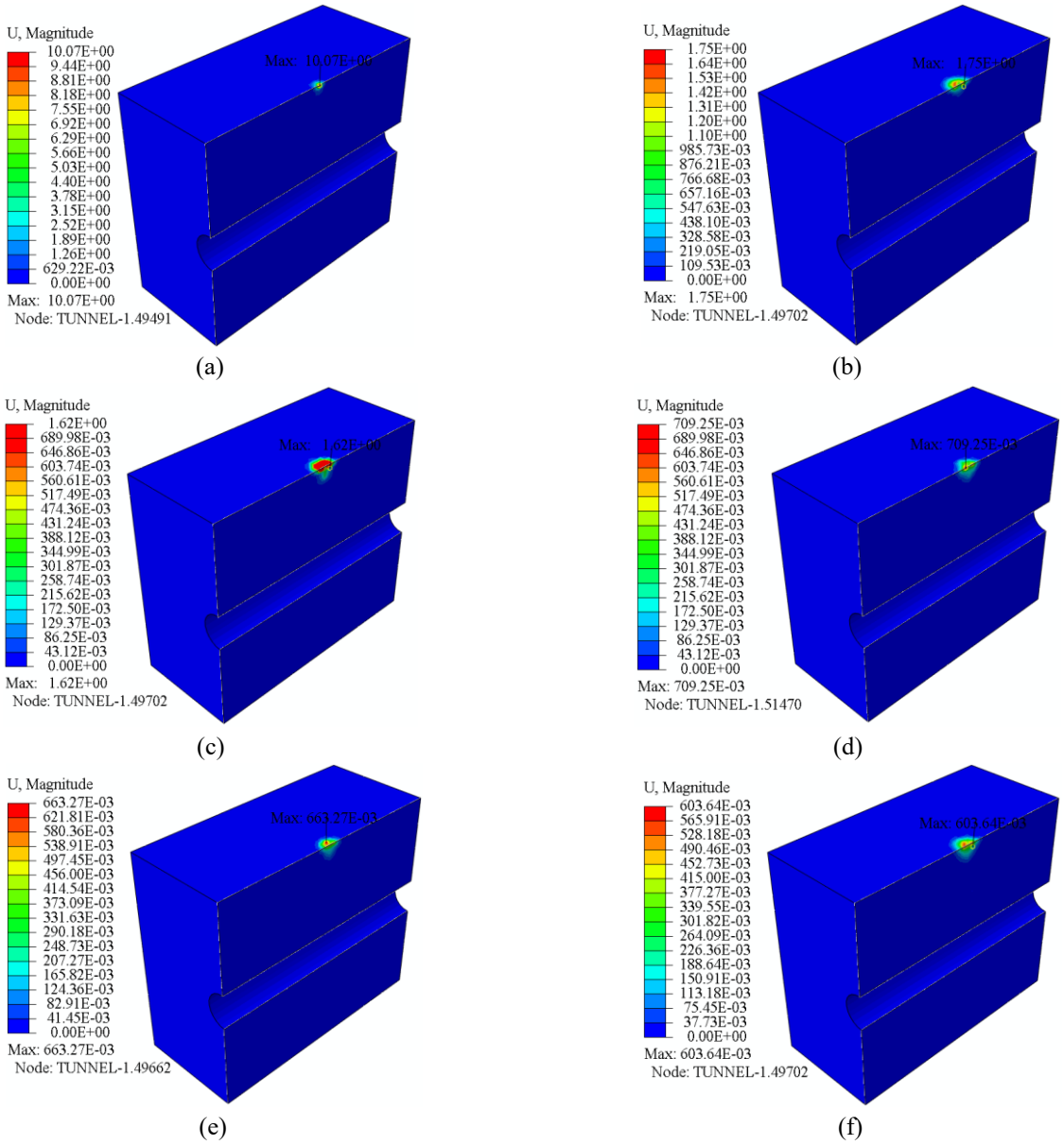

Fig. 9 Deformation Contours of Different Rocks (a) Dolomite, (b) Shale, (c) Sandstone, (d) Granite, (e) Basalt and (f) Quartzite

considered fixed (No translational and rotational movement) at the base, and the top surface is free. Assembly and detailed boundary conditions are shown in Fig. 6.

The general hard contact has been considered and applied as a contact property. Mesh convergence and boundary convergence studies were performed to identify an appropriate mesh density. The global meshing size for rock mass taken was 0.008 selected based on mesh convergence study, and for hammer global meshing size was 0.004. Mesh convergence study has been performed for GM material of 5cm overburden under 17.4kg drop load. A similar analysis has been done using different mesh sizes and deformation under the drop load has been captured. The deformation of the tunnel with varying mesh sizes is shown in Fig. 7. Therefore, it was observed that finer mesh size than 0.008 does not affect too much deformation of the tunnel. C3D8R element type has been considered for meshing which is same as considered in the present study for tunnel. The final meshed parts of the model are shown in Fig. 8. The boundary conditions are same as reported by Sharma *et al.* (2018) for the impact loading model used for validation.

Table 6 shows the comparison of deformation at the tunnel crown when GM and POP rock tunnel has been subjected to impact loading due to different weights of the hammer. Moreover, it has been observed that results from the experimental and numerical study are close, therefore, the present numerical model is validated.

4. Results and discussion

The present paper deals with the study of impact loading on the rock tunnel having a varying range of unconfined

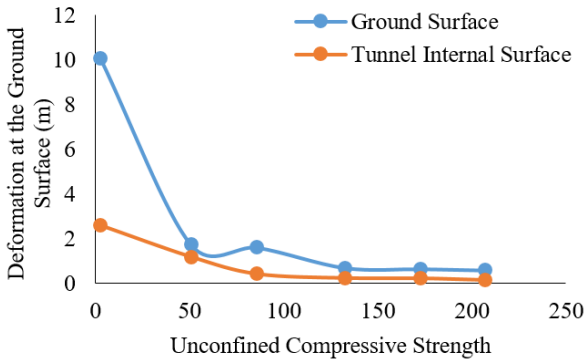

Fig. 10 Variation of deformation for UCS of rock mass surrounding the tunnel

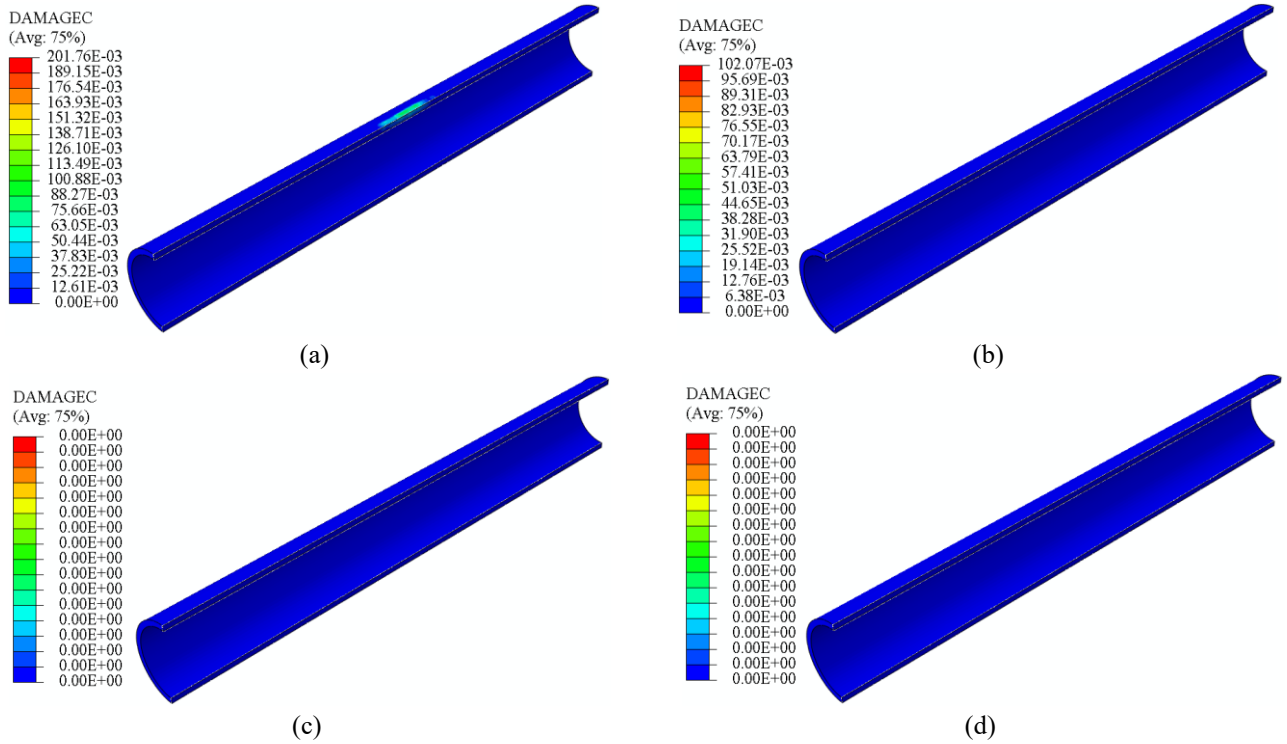

Fig. 11 Compression damage contours for different grades of concrete in case of Dolomite rock (a) M20, (b) M30, (c) M40 and (d) M50 having reinforcement of Fe250 grade

compressive strength (UCS). The finite element analysis has been carried out using Abaqus/Explicit. Moreover, different grades of concrete, i.e., M20, M30, M40, and M50, were adopted, and Fe250, Fe415, and Fe500 grades of steel were used for steel bars used as reinforcement in the tunnel lining. The results obtained by the present simulation are presented as contours and graphs. Further, the results are presented and discussed in the present section.

Fig. 9 shows the deformation contours of the rock tunnel having varying UCS of rock surrounding the tunnel. These results are shown for the maximum value of deformation when the simulation has been carried out for 0.03 seconds. It has been noted that the UCS value of rock also contributed to the impact-resistant designing of an underground rock tunnel. Moreover, the impact load shows maximum deformation, i.e., 10.07 m in Dolomite, while this value keeps on decreasing with an increase in UCS value of rock. The value of deformation noted for an impact loading in Shale, Sandstone, Granite, Basalt, and Quartzite tunnel is 1.75 m, 1.62 m, 0.709 m, 0.663 m, and 0.603 m respectively. Therefore, it has been observed that if the weakest rock is surrounding the tunnel (lowest UCS value of rock), then the impact load has a maximum effect while lesser damage has been transferred to the rock tunnel in case of the higher value of UCS.

The deformations observed at the ground surface and the internal surface of the tunnel are compared in Fig. 10 for a varying range of UCS of rock. It has been noted that UCS of rock and the deformation in the tunnel and at the ground surface are inversely proportional. Therefore, rock mass having the lowest value of UCS has maximum deformations, i.e., in the case of Dolomite. In contrast, minimum deformations were observed for the rock tunnel having the highest value of UCS.

There are two major types of failures in concrete, i.e., compression failure and tension failure. These failures are shown in Figs. 11 and 12 for compression and tension

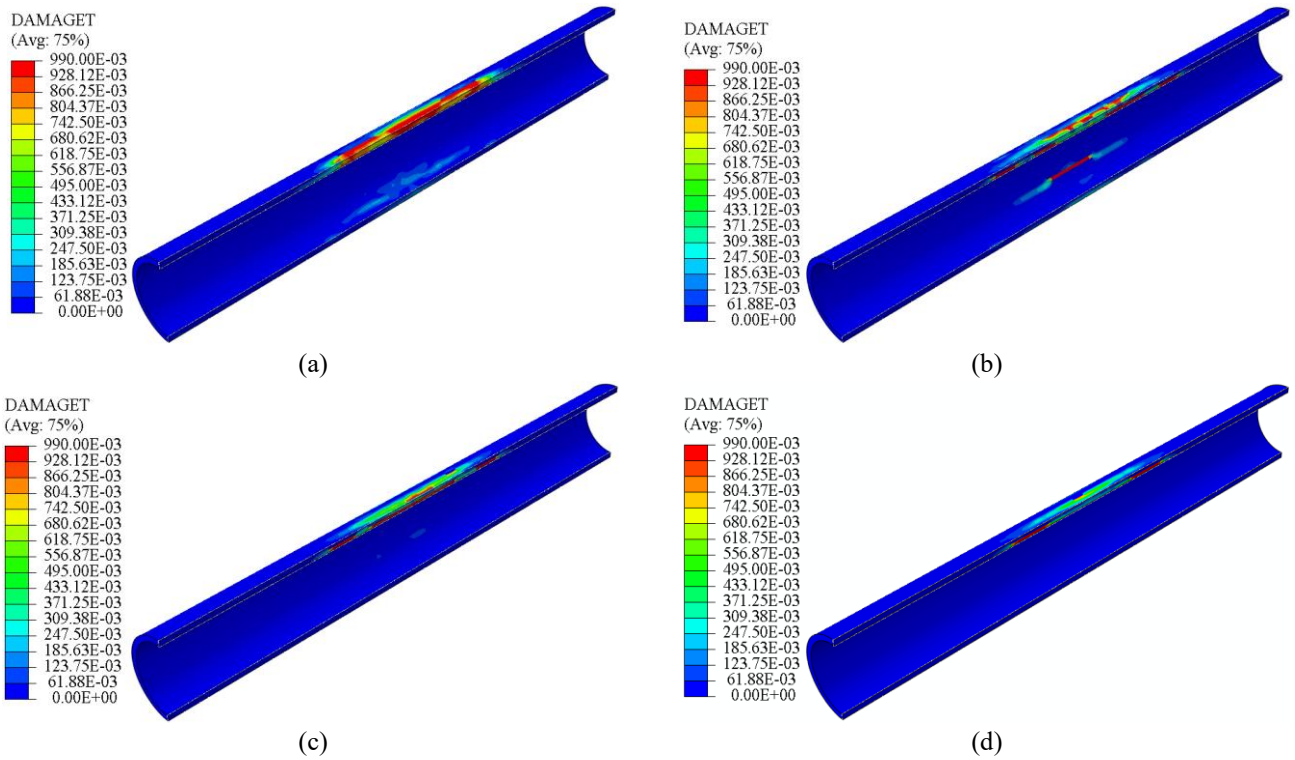

Fig. 12 Tension damage contours for different grades of concrete in case of Dolomite rock (a) M20, (b) M30, (c) M40 and (d) M50 having reinforcement of Fe250 grade

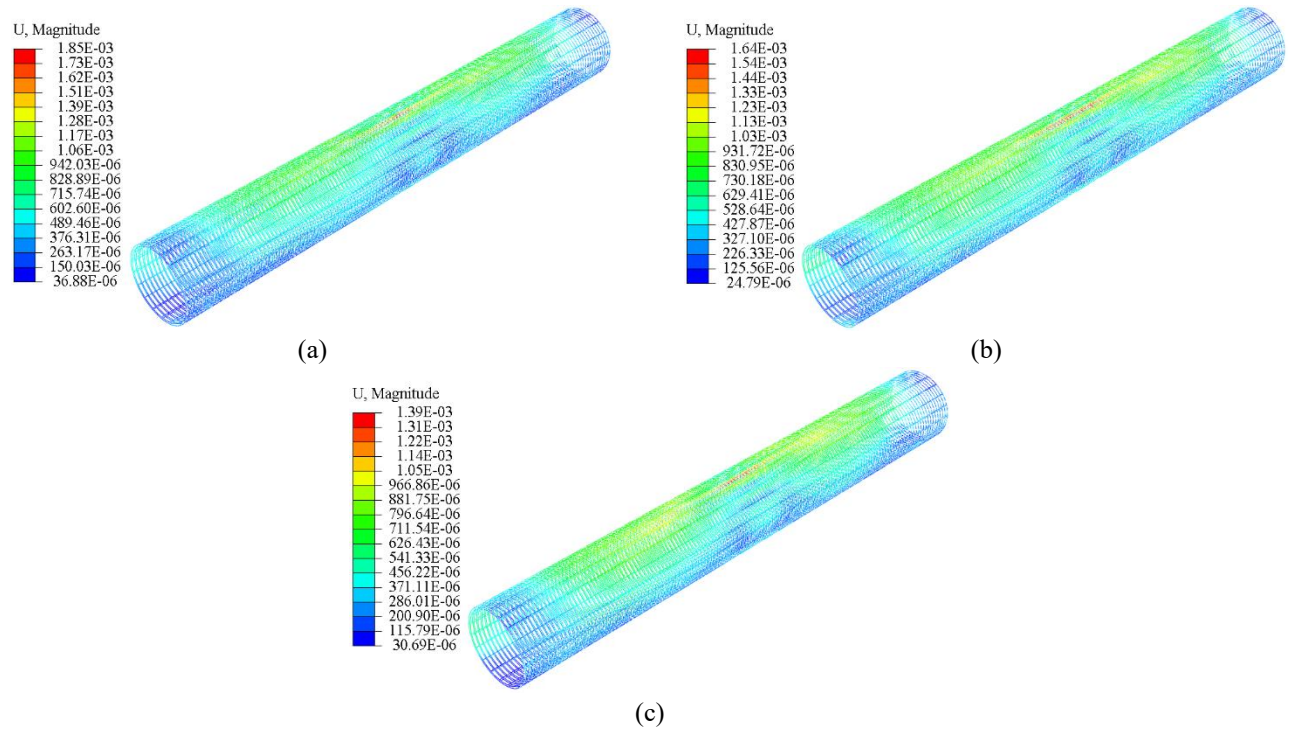

Fig. 13 Deformation contours in case of M20 grade concrete liner having Dolomite rock for different steel grades (a) Fe250, (b) Fe415 and (c) Fe500

failures, respectively. These damage contours are shown for M20, M30, M40 and M50 grades of concrete having steel reinforcement of Fe250 grade in case of Dolomite. It has been observed that M40 and M50 grades of concrete liners are the impact-resistant grades of liners, while 20% and 10% of failure has been observed in the case of M20 and M30 grade of the liner. Moreover, tension failure of the concrete liner has been observed in all the grades of concrete at the crown. However, the tension damage decreases in a higher grade of concrete liners. The primary

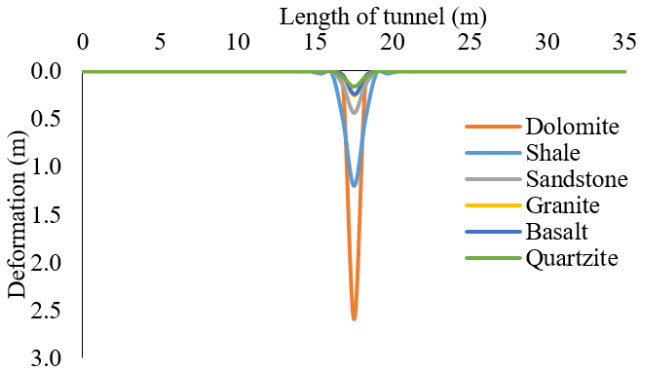

Fig. 14 Deformation profile of different rocks when subjected to impact loading

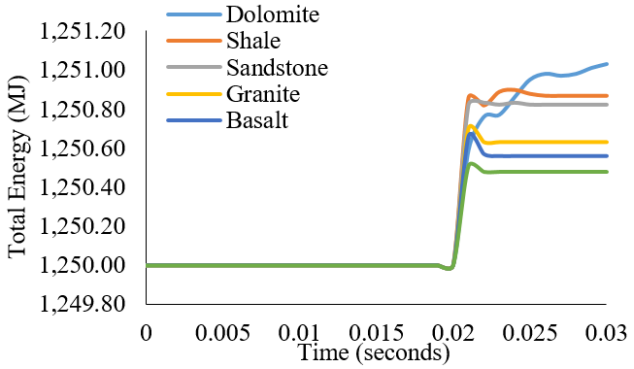

Fig. 15 Time variation of total energy for comparing the different rock having Fe250 grade steel and M20 grade concrete when subjected to impact loading

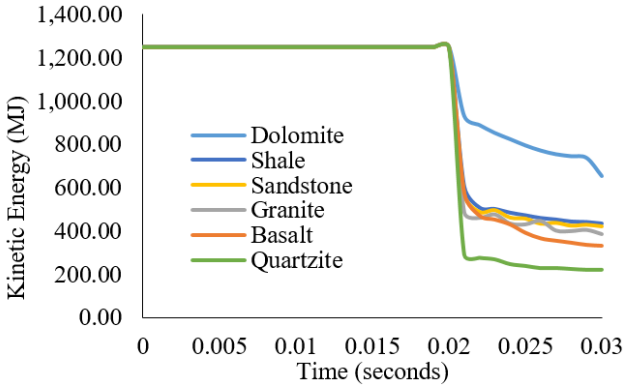

Fig. 16 Time variation of kinetic energy for comparing the different rock having Fe250 grade steel and M20 grade concrete when subjected to impact loading

reason for such a behaviour is the increase of concrete strength of high grades. Furthermore, the length of tension failure having 99% failure is maximum in the M20 grade of concrete while it decreases for M50 grade of the concrete liner. Thus, the M40 grade of concrete can be used for the impact-resistant design of the underground rock tunnels.

Fig. 13 shows the deformation contours for different steel grades, i.e., Fe250, Fe415, and Fe500, which has been used as reinforcement in the concrete liner. The maximum deformation has been observed in Fe250 grade steel, i.e., 1.85mm, while 1.64mm and 1.39mm of deformation have been observed for Fe415 and Fe500 grade of steel. Therefore, the grade of steel reinforcement, which has been used as a reinforcing bar in concrete liner, has a significant effect. However, the difference in the deformation is negligible. Therefore, the grade of steel reinforcement used in the impact-resistant design has no significant effect. Nevertheless, the effect of the diameter of the reinforcing bar may be studied and can be taken up as a separate study.

The deformation profile of the tunnel along the length has been plotted for different rocks in Fig. 14. The deformation shows inverse relation with the UCS of the rock. Moreover, it has been observed that rock tunnel having Dolomite, is the most critical case having maximum penetration of missile. However, Quartzite, Basalt, and Granite tunnels proved much safer than others, and the Quartzite tunnel posses the safest case among the adopted rocks.

The total energy released during the dynamic loading for different rock tunnels is also an essential criterion for the comparison response of rock tunnel with varying UCS, as shown in Fig. 15. The range of total energy for all the rocks adopted in the present study is very narrow. By comparing the different cases of rock tunnel when subjected to impact loading, it has been observed that weaker rocks absorb a higher amount of energy. While, as the strength of the rock increases, i.e., UCS of rock increases, it has been found that the amount of total energy released during an impact loading reduces. Moreover, a slight peak has been observed in all the cases as the missile impacts the ground surface of the rock tunnel. After which the total energy becomes constant.

Fig. 16 shows the variation of total kinetic energy with time for comparing the different rocks having an M20 grade of the concrete liner with Fe250 grade of steel. Maximum kinetic energy has been observed as the missile starts from its initial position, and it keeps on decreasing after hitting the ground surface. From the graph, it has been concluded that the kinetic energy is directly proportional to the unconfined compressive strength (UCS). Therefore, the Dolomite tunnel has the highest value of kinetic energy, and the Quartzite rock tunnel shows the lowest value of kinetic energy. Thus, making the Quartzite rock tunnel to be the most suitable choice for the impact-resistant design of the tunnel.

Strain energy released during an impact loading on the rock tunnel having concrete liner of M20 grade and steel reinforcement of Fe250 grade in all the different cases of rocks is plotted in Fig. 17. It has been observed that strain energy is inversely related to the UCS of the rock. As the Dolomite rock, having the lowest value of UCS has maximum strain energy released in comparison to all the rock. The lowest strain energy has been released in the case of a Quartzite rock tunnel. Since the Dolomite rock tunnel has maximum penetration of the missile and thus, it has maximum strain energy released. The strain energy increases as the missile penetrates, while after reaching the maximum penetration, the strain energy value keeps on decreasing. Also, it has been concluded that impact resistance is higher when the UCS of rock is higher from the strain energy plot.

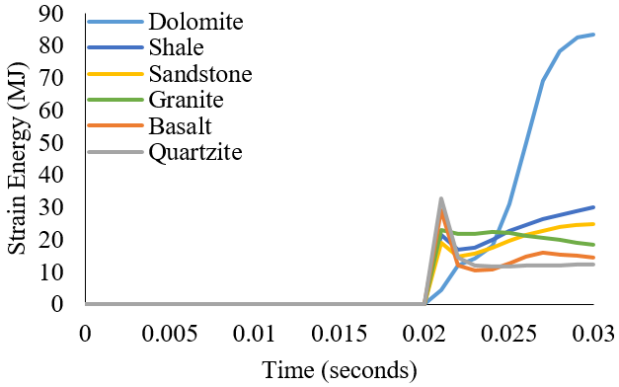

Fig. 17 Time variation of strain energy for comparing the different rock having Fe250 grade steel and M20 grade concrete when subjected to impact loading

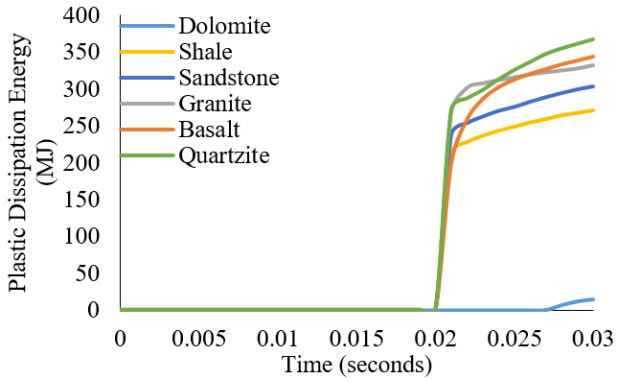

Fig. 18 Time variation of plastic dissipation energy for comparing the different rock having Fe250 grade steel and M20 grade concrete when subjected to impact loading

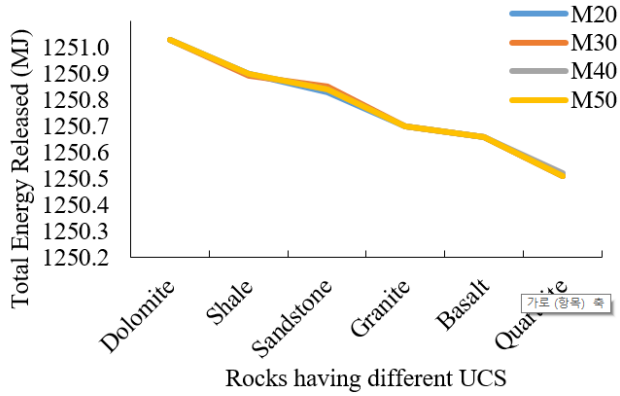

Fig. 19 Variation of the total energy released for increasing value of UCS having Fe250 grade of steel for different grades of the concrete liner

Fig. 18 has been plotted for the comparison of different rocks for the plastic dissipation energy. The plot is shown for different rocks having an M20 grade of the concrete liner of the tunnel that has been reinforced with Fe250 grade of steel bars. From the graphs, it has been concluded that plastic dissipation energy is directly proportional to the UCS of the rock surrounding the tunnel. At the last time, that is 0.03 seconds; it has been noted that Dolomite tunnels

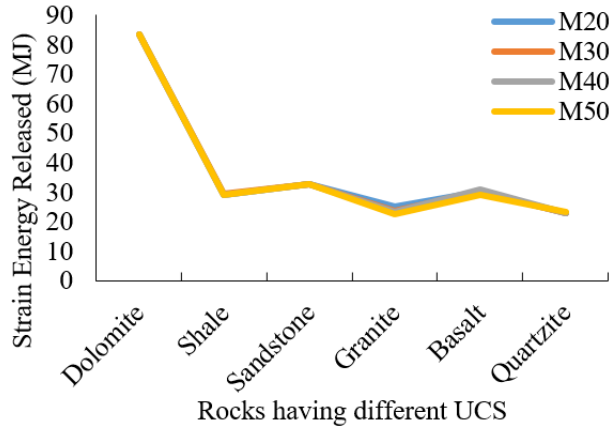

Fig. 20 Variation of strain energy released for increasing value of UCS having Fe250 grade of steel for different concrete liner grade

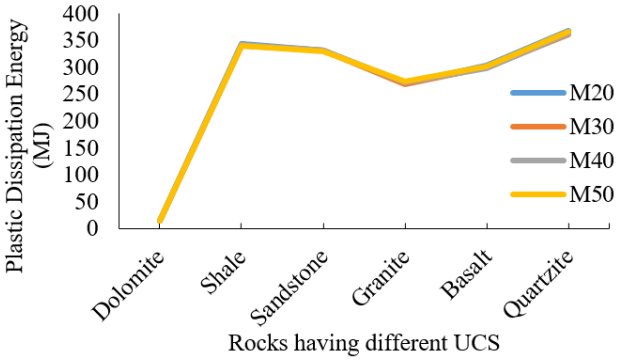

Fig. 21 Variation of plastic dissipation energy released for increasing value of UCS having Fe250 grade of steel for different concrete liner grade

are the most unsuitable choice for the impact-resistant design of the tunnel. However, Quartzite rock tunnels are the most suitable choice for the impact-resistant design. In other words, higher the value of UCS of rock, better impact resistant behaviour is observed. Therefore, the UCS of the rock should be taken into account while designing the rock tunnels for impact-resistant design.

Fig. 19 has been plotted for the comparison of the total energy released during an impact loading event. It has been analyzed for different rocks in case of varying grades of concrete for steel reinforcement having Fe250 grade. It has been noted that the total energy released decreases with an increase in the UCS of the rock in which the tunnel has been constructed. Moreover, the response of all the rocks remains similar for all the different grades of the concrete liner having a steel reinforcement grade of Fe250. The linearly decreasing graph has been observed for total energy released for increasing UCS of rock. The reason for this behaviour is that as the strength of the rock increases, the energy released in the different cases changes depending upon the UCS of the rock surrounding the tunnel.

The strain energy released during an impact loading is an essential parameter for comparing the different rocks. From the relation between the strain energy and the UCS of the different rock mass surrounding the tunnel, it has been

observed that the UCS of the rock has a significant effect on the strain energy released. Moreover, it has been observed that as the UCS of the rock mass surrounding the tunnel increases, the strain energy released keeps on decreasing, thus making the highest UCS rock the most resistant to impact loading. Fig. 20 has been plotted for the comparison of strain energy released in different grades of concrete, having steel reinforcement of Fe250 grade to understand the UCS relation with strain energy released.

The variation of plastic dissipation energy has been plotted in Fig. 21 for varying UCS value of surrounding rock mass for different grades of concrete liners having Fe250 grade of steel reinforcement. From the graph, it has been observed that with the increase in UCS value of rock mass surrounding the tunnel, the value of plastic dissipation energy increases. The primary reason for this increase in the energy found to be due to increasing strength. Since, in the case of the weakest rock, the missile has maximum penetration. Therefore, lesser energy has been consumed in resisting missile penetration. Hence, it has been concluded that with the increase in the value of UCS, the impact-resisting strength increases.

5. Conclusions

This study has been carried out to understand the response of rock tunnels when subjected to impact loading conditions. The finite element technique has been adopted for the validation of this numerical technique and different analyses. The parameters varied in this study include UCS of rock, the grade of the concrete liner, and the grade of steel. It has been observed that these parameters have a significant effect on the stability of rock tunnels against impact load. Some significant points concluded from the present study are:

1. The tunnel constructed in Dolomite has 5.75-times lesser safety and serviceability against impact load in comparison to Shale since the Shale has 17.86-times higher value of UCS than Dolomite. Moreover, the Quartzite rock tunnel has 16.68-times more impact-resisting strength than Dolomite because the Quartzite has a higher value of UCS among the different rocks considered in the present study. Therefore, deformations caused by an impact load are inversely proportional to the UCS of rock in which the tunnel has been constructed.

2. The missile has penetrated to a higher depth in the case of Dolomite, while its depth reduces with an increase in the UCS value. The damage in the concrete is directly proportional to the depth of penetration of the missile. Therefore, the M40 grade of concrete has been found as the most suitable choice for the impact-resisting design of tunnel lining.

3. The energy released by the whole finite element model during an impact loading event also has a significant influence on the impact resistance design and analysis of rock tunnel. The grade of steel and concrete has a lesser significant effect on the energy released due to the impact load by a missile. The energy released is inversely proportional to the UCS of rock; however, its variation with time has been influenced by the value of UCS.

References

Abaqus, (2019), *ABAQUS User's Manual*, Dassault Systems.

Abramson, L.W., Hansmire, W.H. and Boyce, G.M. (1993), "Performance of tunnel portals in weathered rock", *Int. J. Rock Mech. Min. Sci.*, **30**(7), 1449-1452. https://doi.org/10.1016/0148-9062(93)90136-2.

Arias, D., Pando, L., López-Fernández, C., Díaz-Díaz, L.M. and Rubio-Ordóñez, Á. (2016), "Deep weathering of granitic rocks: A case of tunnelling in NW Spain", *Catena*, **137**, 572-580. https://doi.org/10.1016/j.catena.2015.10.026.

Azizi, F., Koopialipoor, M. and Khoshrou, H. (2019), "Estimation of rock mass squeezing potential in tunnel route (Case Study: Kerman water conveyance tunnel)", *Geotech. Geol. Eng.*, **37**(3), 1671-1685. https://doi.org/10.1007/s10706-018-0714-5.

Buonsanti, M. and Leonardi, G. (2013), "3-D simulation of tunnel structures under blast loading", *Arch. Civ. Mech. Eng.*, **13**(1), 128-134. https://doi.org/10.1016/j.acme.2012.09.002.

Chen, L., Zhou, Z., Zang, C., Zeng, L. and Zhao, Y. (2019), "Failure pattern of large-scale goaf collapse and a controlled roof caving method used in gypsum mine", *Geomech. Eng.*, **18**(4), 449-457. https://doi.org/10.12989/gae.2019.18.4.449.

Chu, Z., Wu, Z., Liu, B. and Liu, Q. (2019), "Coupled analytical solutions for deep-buried circular lined tunnels considering tunnel face advancement and soft rock rheology effects", *Tunn. Undergr. Sp. Tech.*, **94**, 103111. https://doi.org/10.1016/j.tust.2019.103111.

Do, T.N. and Wu, J.H. (2020), "Verifying discontinuous deformation analysis simulations of the jointed rock mass behavior of shallow twin mountain tunnels", *Int. J. Rock Mech. Min. Sci.*, **130**, 104322. https://doi.org/10.1016/j.ijrmms.2020.104322.

Feldgun, V.R., Kochetkov, A. V., Karinski, Y.S. and Yankelevsky, D.Z. (2008), "Internal blast loading in a buried lined tunnel", *Int. J. Impact Eng.*, **35**, 172-183. https://doi.org/10.1016/j.ijimpeng.2007.01.001.

Goel, M.D., Matsagar, V. and Marburg, S. (2011), "An abridged review of blast wave parameters", *Defence Sci. J.*, **62**(5), 300-306.

Gschwandtner, G.G. and Galler, R. (2013), "Laugungsversuche als Grundlage zur Stabilitätsuntersuchung von Grubengebäuden in wasserlöslichen Gebirgsformationen [Leaching Experiments as Basis for the Stability Analysis of Underground Structures in Water-Soluble Rock Formations]", *BHM Berg- und Hüttenmännische Monatshefte*, **158**, 493-500. https://doi.org/10.1007/s00501-013-0202-4.

Gupta, A.S. (1997), "Engineering behavior and classification of weathering rock", Indian Institute of Technology Delhi, Delhi, India.

Gurocak, Z. and Yalcin, E. (2016), "Excavatability and the effect of weathering degree on the excavatability of rock masses: An example from Eastern Turkey", *J. African Earth Sci.*, **118**, 1-11. https://doi.org/10.1016/j.jafrearsci.2016.02.017.

Hafezolghorani, M., Hejazi, F., Vaghei, R., Jaafar, M.S.B. and Karimzade, K. (2015), "Simplified damage plasticity model for concrete", *Struct. Eng. Int.*, **27**(1), 68-78. https://doi.org/10.2749/101686616X1081.

Han, Y. and Liu, H. (2016), "Failure of circular tunnel in saturated soil subjected to internal blast loading", *Geomech. Eng.*, **11**(3), 421-438. https://doi.org/10.12989/gae.2016.11.3.421.

Han, Y., Zhang, L. and Yang, X. (2016), "Soil-tunnel interaction under medium internal blast loading", *Procedia Eng.*, **143**, 403-410. https://doi.org/10.1016/j.proeng.2016.06.051.

Huang, F., Wu, C., Jang, B.A., Hong, Y., Guo, N. and Guo, W.

(2020), "Instability mechanism of shallow tunnel in soft rock subjected to surcharge loads", *Tunn. Undergr. Sp. Tech.*, **99**, 103350. https://doi.org/10.1016/j.tust.2020.103350.

Huang, X., Zhang, J., Yang, L., Yang, S. and Wang, X. (2016), "Elasto-plastic analysis of the surrounding rock mass in circular tunnel based on the generalized nonlinear unified strength theory", *Int. J. Min. Sci. Technol.*, **26**(5), 819-823. https://doi.org/10.1016/j.ijmst.2016.05.043.

IS456 (2000), Plain and Reinforced Concrete - Code of Practice, Parliament of India, New Delhi, India.

Jeon, S., Kim, T.H. and You, K.H. (2015), "Characteristics of crater formation due to explosives blasting in rock mass", *Geomech. Eng.*, **9**(3), 329-344. https://doi.org/10.12989/gae.2015.9.3.329.

Johnson, G.R. and Cook, W.H. (1983), "A constitutive model and data for materials subjected to large strains, high strain rates, and high temperatures", *Proceedings of 7th International Symposium on Ballistics*, Hague, The Netherlands, April.

Kargar, A.R. (2019), "An analytical solution for circular tunnels excavated in rock masses exhibiting viscous elastic-plastic behaviour", *Int. J. Rock Mech. Min. Sci.*, **124**, 104128. https://doi.org/10.1016/j.ijrmms.2019.104128.

Kim, D. and Park, K. (2019), "Study on the characteristics of grout material using ground granulated blast furnace slag and carbon fiber", *Geomech. Eng.*, **19**(4), 361-368. https://doi.org 10.12989/gae.2019.19.4.361.

Koneshwaran, S., Thambiratnam, D.P. and Gallage, C. (2015), "Blast response of segmented bored tunnel using coupled SPH-FE method", *Structures*, **2**, 58-71. https://doi.org/10.1016/j.istruc.2015.02.001.

Kristoffersen, M., Minoretti, A. and Børvik, T. (2019), "On the internal blast loading of submerged floating tunnels in concrete with circular and rectangular cross-sections", *Eng. Fail. Anal.*, **103**, 462-480. https://doi.org/10.1016/j.engfailanal.2019.04.074.

Kumar, A. (2019), "Engineering behavior of oil shale under high pressure after thermal treatment", Ph.D. Thesis, IIT Delhi, Delhi, India.

Lane, K.S. (2019), Tunnels and underground excavations, https://www.britannica.com/technology/tunnel.

Lee, C.J. (2012), "Three-dimensional numerical analyses of the response of a single pile and pile groups to tunnelling in weak weathered rock", *Tunn. Undergr. Sp. Tech.*, **32**, 132-142. https://doi.org/10.1016/j.tust.2012.06.005.

Li, C. and Li, X. (2018), "Influence of wavelength-to-tunnel-diameter ratio on dynamic response of underground tunnels subjected to blasting loads", *Int. J. Rock Mech. Min. Sci.*, **112**, 323-338. https://doi.org/10.1016/j.ijrmms.2018.10.029.

Li, X., Li, C., Cao, W. and Tao, M. (2018), "Dynamic stress concentration and energy evolution of deep-buried tunnels under blasting loads", *Int. J. Rock Mech. Min. Sci.*, **104**, 131-146. https://doi.org/10.1016/j.ijrmms.2018.02.018.

Limited, D.M.R.C., (2015), *Design Specifications*, Barakhamba road, New Delhi, India.

Liu, Q., Xu, X. and Wu, Z. (2020), "A GPU-based numerical manifold method for modeling the formation of the excavation damaged zone in deep rock tunnels", *Comput. Geotech.*, **118**, 103351. https://doi.org/10.1016/j.compgeo.2019.103351.

Lubliner, J., Oliver, J., Oller, S. and Oñate, E. (1989), "A plastic-damage model for concrete", *Int. J. Solids Struct.*, **25**(3), 299-326. https://doi.org/10.1016/0020-7683(89)90050-4.

McQueen, L.B., Purwodihardjo, A. and Barrett, S.V.L. (2019), "Rock mechanics for design of Brisbane tunnels and implications of recent thinking in relation to rock mass strength", *J. Rock Mech. Geotech. Eng.*, **11**(3), 676-683. https://doi.org/10.1016/j.jrmge.2019.02.001.

Mishra, S. (2019), "Physical and numerical modeling of tunnels under impact and blast loads", Ph.D. Thesis, IIT Delhi, Delhi, India.

Mishra, S., Rao, S., Gupta, N.K. and Kumar, A. (2018), "Damage to shallow tunnels in different geomaterials under static and dynamic loading", *Thin-Walled Struct.*, **126**, 138-149.

Mitelman, A. and Elmo, D. (2014), "Modelling of blast-induced damage in tunnels using a hybrid finite-discrete numerical approach", *J. Rock Mech. Geotech. Eng.*, **6**(6), 565-573. https://doi.org/10.1016/j.jrmge.2014.09.002.

Naqvi, M.W., Akhtar, M.F., Zaid, M. and Sadique, M.R. (2021), "Effect of superstructure on the stability of underground tunnels", *Transp. Infrastruct. Geotechnol.*, 1-20. https://doi.org/10.1007/s40515-020-00119-6.

Ozacar, V. (2018), "New methodology to prevent blasting damages for shallow tunnel", *Geomech. Eng.*, **15**(6), 1227-1236. https://doi.org/10.12989/gae.2018.15.6.1227.

Park, D. and Michalowski, R.L. (2020), "Three-dimensional roof collapse analysis in circular tunnels in rock", *Int. J. Rock Mech. Min. Sci.*, **128**, 104275. https://doi.org/10.1016/j.ijrmms.2020.104275.

Pojani, D. and Stead, D. (2015), "Sustainable urban transport in the developing world: Beyond megacities", *Sustainability*, **7**, 7784-7805. https://doi.org/10.3390/su7067784.

Qin, C.B., Yang, X.L., Pan, Q.J., Sun, Z.B., Wang, L.L. and Miao, T. (2015), "Upper bound analysis of progressive failure mechanism of tunnel roofs in partly weathered stratified Hoek-Brown rock masses", *Int. J. Rock Mech. Min. Sci.*, **74**, 157-162. https://doi.org/10.1016/j.ijrmms.2014.10.002.

Rahaman, O. and Kumar, J. (2020), "Stability analysis of twin horse-shoe shaped tunnels in rock mass", *Tunn. Undergr. Sp. Tech.*, **98**, 103354. https://doi.org/10.1016/j.tust.2020.103354.

Rasmussen, L.L., Cacciari, P.P., Futai, M.M., de Farias, M.M. and de Assis, A.P. (2019), "Efficient 3D probabilistic stability analysis of rock tunnels using a Lattice Model and cloud computing", *Tunn. Undergr. Sp. Tech.*, **85**, 282-293. https://doi.org/10.1016/j.tust.2018.12.022.

Sharma, H., Mishra, S., Rao, K.S. and Gupta, N.K. (2018), "Effect of cover depth on deformation in tunnel lining when subjected to impact load", *Proceedings of the 10th Asian Rock Mechanics Symposium*, Singapore.

Shi, C., Zhao, Q., Lei, M. and Peng, M. (2019), "Vibration velocity control standard of buried pipeline under blast loading of adjacent tunnel", *Soils Found.*, **59**, 2195-2205. https://doi.org/10.1016/j.sandf.2019.12.003.

Shirlaw, J.N. (2016), "Pressurised TBM tunnelling in mixed face conditions resulting from tropical weathering of igneous rock", *Tunn. Undergr. Sp. Tech.*, **57**, 1-16. https://doi.org/10.1016/j.tust.2016.01.018.

Shrestha, G.L. and Broch, E. (2008), "Influences of the valley morphology and rock mass strength on tunnel convergence: With a case study of Khimti 1 headrace tunnel in Nepal", *Tunn. Undergr. Sp. Tech.*, **23**(6), 638-650. https://doi.org/10.1016/j.tust.2007.12.006

Sofianos, A.I. and Nomikos, P.P. (2006), "Equivalent Mohr-Coulomb and generalized Hoek-Brown strength parameters for supported axisymmetric tunnels in plastic or brittle rock", *Int. J. Rock Mech. Min. Sci.*, **43**, 683-704. https://doi.org/10.1016/j.ijrmms.2005.11.006.

Song, K.I., Cho, G.C. and Lee, S.W. (2011), "Effects of spatially variable weathered rock properties on tunnel behaviour", *Probabilist. Eng. Mech.*, **26**(3), 413-426. https://doi.org/10.1016/j.probengmech.2010.11.010.

Song, Z.P., Li, S.H., Wang, J.B., Sun, Z.Y., Liu, J. and Chang, Y.Z. (2018), "Determination of equivalent blasting load considering millisecond delay effect", *Geomech. Eng.*, **15**(2), 745-754. https://doi.org/10.12989/gae.2018.15.2.745.

Systemes, D. (2014), Abaqus 6.14 Documentation, Dassault Systèmes, Providence, Rhode Island, U.S.A.

Uyar, G.H. and Aksoy, C.O. (2019), "Comparative review and interpretation of the conventional and new methods in blast vibration analyses", *Geomech. Eng.*, **18**(5), 545-554. https://doi.org/10.12989/gae.2019.18.5.545.

Vidanović, N., Rašuo, B., Kastratović, G., Maksimović, S., Ćurčić, D. and Samardžić, M. (2017), "Aerodynamic-structural missile fin optimization", *Aerosp. Sci. Technol.*, **65**, 26-45. https://doi.org/10.1016/j.ast.2017.02.010.

Wang, X. and Cai, M. (2020), "A DFN-DEM multi-scale modeling approach for simulating tunnel excavation response in jointed rock masses", *Rock Mech. Rock Eng.*, **53**, 1053-1077. https://doi.org/10.1007/s00603-019-01957-8.

Xia, Q., Zhang, L., Dong, H., Li, Z., Zhang, Y., Hu, J., Chen, H. and Chen, Y. (2020), "Bio-weathering of a uranium-bearing rhyolitic rock from Xiangshan uranium deposit, Southeast China", *Geochim. Cosmochim. Acta*, **279**, 88-106. https://doi.org/10.1016/j.gca.2020.03.044.

Xiang, Y. and Yang, Y. (2017), "Spatial dynamic response of submerged floating tunnel under impact load", *Mar. Struct.*, **53**, 20-31. https://doi.org/10.1016/j.marstruc.2016.12.009.

Yang, G., Wang, G., Lu, W., Yan, P. and Chen, M. (2019), "Damage assessment and mitigation measures of underwater tunnel subjected to blast loads", *Tunn. Undergr. Sp. Tech.*, **94**, 103131. https://doi.org/10.1016/j.tust.2019.103131.

Yang, J., Cai, J., Yao, C., Li, P., Jiang, Q. and Zhou, C. (2019), "Comparative study of tunnel blast-induced vibration on tunnel surfaces and inside surrounding rock", *Rock Mech. Rock Eng.*, **52**(11), 4747-4761. https://doi.org/10.1007/s00603-019-01875-9.

Zaid, M. and Mishra, S. (2021), "Numerical analysis of shallow tunnels under static loading: A finite element approach", *Geotech. Geol. Eng.*, 1-27. https://doi.org/10.1007/s10706-020-01647-1

Zaid, M. and Rehan Sadique, M. (2021a), *Dynamic Analysis of Tunnels in Western Ghats of Indian Peninsula: Effect of Shape and Weathering*, in *Recent Trends in Civil Engineering*, Springer, Singapore, 763-776.

Zaid, M. and Rehan Sadique, M. (2021b), "A simple approximate simulation using coupled Eulerian-Lagrangian (CEL) simulation in investigating effects of internal blast in rock tunnel", *Indian Geotech. J.*, 1-18. https://doi.org/10.1007/s40098-021-00511-0.

Zaid, M. and Sadique, M.R. (2020a), "Blast resistant behaviour of tunnels in sedimentary rocks", *Int. J. Prot. Struct.* https://doi.org/10.1177/2041419620951211.

Zaid, M. and Sadique, M.R. (2020b), "The response of rock tunnel when subjected to blast loading: Finite element analysis", *Eng. Reports*. https://doi.org/10.1002/eng2.12293.

Zaid, M., Mishra, S. and Rao, K.S. (2019a), "Stability of different shapes of Himalayan tunnels under blast loading", *Proceedings of the 8th Indian Rock Conference*, New Delhi, India.

Zaid, M., Mishra, S. and Rao, K.S. (2020a), *Finite Element Analysis of Static Loading on Urban Tunnels.*, in *Geotechnical Characterization and Modelling*, Springer, Singapore, 807-823.

Zaid, M., Sadique, M.R. and Alam, M.M. (2021), "Blast analysis of tunnels in Manhattan-Schist and Quartz-Schist using coupled-Eulerian-Lagrangian method", *Innov. Infrastruct. Solut.*, **6**(2), 1-10. https://doi.org/10.1007/s41062-020-00446-0.

Zaid, M., Sadique, M.R. and Samanta, M. (2020b), "Effect of unconfined compressive strength of rock on dynamic response of shallow unlined tunnel", *SN Appl. Sci.*, **2**(12), 1-13. https://doi.org/10.1007/s42452-020-03876-8.

Zaid, M., Shah, I.A. and Farooqi, M.A. (2019b), "Effect of cover depth in unlined Himalayan Tunnel: A finite element approach", *Proceedings of the 8th Indian Rock Conference*, New Delhi, India.

Zareifard, M.R. (2020), "A new semi-numerical method for elastoplastic analysis of a circular tunnel excavated in a Hoek-Brown strain-softening rock mass considering the blast-induced damaged zone", *Comput. Geotech.*, **122**, 103476. https://doi.org/10.1016/j.compgeo.2020.103476.

Zhang, J.Z., Zhou, X.P. and Yin, P. (2019), "Visco-plastic deformation analysis of rock tunnels based on fractional derivatives", *Tunn. Undergr. Sp. Tech.*, **85**, 209-219. https://doi.org/10.1016/j.tust.2018.12.019.

Zhao, Y., Yang, H., Chen, Z., Chen, X., Huang, L. and Liu, S. (2019), "Effects of jointed rock mass and mixed ground conditions on the cutting efficiency and cutter wear of tunnel boring machine", *Rock Mech. Rock Eng.*, **52**, 1303-1313. https://doi.org/10.1007/s00603-018-1667-y.

Zhou, L., Zhu, Z., Dong, Y., Ying, P. and Wang, M. (2019), "Study of the fracture behavior of mode I and mixed mode I/II cracks in tunnel under impact loads", *Tunn. Undergr. Sp. Tech.*, **84**, 11-21. https://doi.org/10.1016/j.tust.2018.10.018.

Zhou, L., Zhu, Z., Wang, M., Ying, P. and Dong, Y. (2018), "Dynamic propagation behavior of cracks emanating from tunnel edges under impact loads", *Soil Dyn. Earthq. Eng.*, **105**, 119-126. https://doi.org/10.1016/j.soildyn.2017.12.012.

JS